

Supporting Information

Functional Additive Incorporation Enhances the Performance of Semi-Transparent Perovskite Solar Cells

Bhavna Sharma,¹ Krishanu Dey,^{2,} Mohammad Adil Afroz,¹ Henry J. Snaith² and Soumitra Satapathi^{1,3,*}*

¹ Department of Physics, Indian Institute of Technology Roorkee, Roorkee, Uttarakhand-247667, India

² Department of Physics, University of Oxford, Clarendon Laboratory, Parks Road, Oxford OX1 3PU, United Kingdom

³ Center for Sustainable Energy, Indian Institute of Technology Roorkee, Roorkee, Uttarakhand-247667, India

Corresponding Author

* Soumitra Satapathi, Email: soumitra.satapathi@ph.iitr.ac.in

* Krishanu Dey, Email: krishanu.dey@physics.ox.ac.uk

Table of Contents:

- Materials
- Device Fabrication
- Characterizations
- Supplementary Notes
- Figure S1-S14
- Table S1-S6

Materials:

FTO glass substrates of sheet resistance of $7 \Omega \text{ sq}^{-1}$, PbI_2 (99.99% pure), CsI (99.9% pure), PbBr_2 (99.99% pure), TFBSC (99% pure), Molybdenum tri-oxide (MoO_3), and all solvents including anhydrous DMF (99.8% pure), anhydrous DMSO (99.8% pure), anhydrous chlorobenzene (99.8% pure), anhydrous IPA (99.8% pure), were acquired from Sigma-Aldrich. FAI was procured from Greatcell Solar and nickel nitrate hexahydrate ($\text{Ni}(\text{NO}_3)_2 \cdot 6\text{H}_2\text{O}$), C_{60} and bathocuproine (BCP) were purchased from TCI. All other chemicals were used in their received form.

Device Fabrication:

FTO cleaning procedure commenced with soap solution, followed by rinsing with DI water, acetone, and isopropyl alcohol (IPA) for a duration of 20 minutes for each solvent. Subsequently, the FTO substrates were dried and treated with UV-ozone for a duration of 30 minutes. 1M of $\text{Ni}(\text{NO}_3)_2 \cdot 6\text{H}_2\text{O}$ was dissolved in 1M ethylenediamine and 1ml ethylene glycol to prepare the NiO_x precursor solution. The NiO_x (hole transporting layer) solution was spin-coated onto the cleaned FTO substrates at 3500 rpm for a duration of 35 seconds followed by the annealing at 300°C for 1 hour under ambient air conditions. The perovskite $\text{FA}_{0.9}\text{Cs}_{0.1}\text{PbI}_2\text{Br}$ precursor solution was prepared by dissolving FAI, CsI, PbBr_2 and PbI_2 in the appropriate molar ratio using a mixed solvent of DMF and DMSO (8:2, V/V). This perovskite solution was kept for continuous stirring at 70°C overnight. Different concentration of TFBSC precursor was added into the perovskite solution for the modified devices. Then the dissolved perovskite precursor solution was spin coated on the NiO_x coated FTO substrates in a two-step spin-coating process (1000 rpm for 10 sec and 4000 rpm for 30 sec). In the second step of the program, 200 μl of anhydrous chlorobenzene was dripped as an antisolvent after 15 seconds and then the substrates were annealed at 100°C for a duration of 10 minutes. After that 30 nm C_{60} and 8 nm BCP was thermally evaporated onto the perovskite layer. At last, 20 nm Ag followed by 5 nm MoO_3 was thermally deposited using a shadow mask to create an active area of 0.1 cm^2 .

Film Characterization:

Perovskite blend films were characterized by UV-vis absorption using a Cary 4000 UV-Vis spectrophotometer by Agilent Instruments. The XRD patterns of the perovskite films were recorded using a Rigaku Micromax-007HF diffractometer equipped with $\text{Cu-K}\alpha 1$ radiation ($\lambda =$

1.54184 Å). Surface morphology of the perovskite films was examined by FESEM (Carl Zeiss FESEM, Zeiss Gemini 300). PL and TRPL measurements were performed using FLS-1000-xs-t (EDINBURGH INSTRUMENTS) with a Picosecond Pulsed Diode Laser source (EPL) of wavelength 450 nm. PLQE measurements were acquired using a custom-built PLQE setup in an integrating sphere and the samples were photoexcited using a 405 nm laser with 1-sun intensity. TPC measurements were performed on the perovskite films on glass using a home-built setup. Interdigitated gold electrodes with 300 μm spacing were used to establish an electric field ≤ 0.01 V/μm. Samples were illuminated by a 10 Hz pulsed laser with 470 nm wavelength. KPFM measurements were carried out using Glovebox-Integrated Bruker Dimension icon XR setup. XPS and UPS measurements were acquired using PHI 5000 VersaProbe III setup.

Device Characterization:

The J - V characteristics were acquired using a Keithley 2400 source meter under nitrogen atmosphere and the devices were illuminated with a solar simulator (AM 1.5G, 100 mW/cm²) from an IPCE System solar simulator (NR175-9008) by SCIENCETECH. The external quantum efficiency (EQE) was determined using an (PTS-2-IQE) Quantum Efficiency/IPCE System with EQE/IQE under ambient conditions. Electrochemical measurements were carried out with a Autolab PGSTAT302N instrument.

Supplementary Notes:

1. Average life time calculation from TRPL:

The average lifetime (T_{avg}) of the films was computed using the data obtained from curve fitting, using the following equation:

$$T_{\text{avg}} = \frac{A_1 T_1^2 + A_2 T_2^2}{A_1 T_1 + A_2 T_2} \quad \text{Equation-S1}$$

Where A_1 , A_2 are relative amplitudes and T_1 , T_2 are decay lifetimes.

2. Energy level and work function from UPS data can be calculated using the following equations:

$$\Phi = E_{\text{cutoff}} - 21.22 \text{ eV}$$

$$E_{\text{VB}} = \phi - E_{\text{edge}}$$

$$E_{CB} = E_g + E_{VB} \quad \text{Equation-S2}$$

3. V_{CPD} was calculated by the following equation:

$$V_{CPD} = \frac{\phi_{tip} - \phi_s}{-e} \quad \text{Equation-S3}$$

Where V_{CPD} is the measured contact potential difference, Φ_{tip} is the work function of the KPFM cantilever tip and Φ_s is the work function of the wide-bandgap perovskite thin-film, and e is the elementary charge.

4. AVT calculation:

AVT of the ST-PSCs can be expressed as follows:

$$AVT (\%) = \frac{\int_{400 \text{ nm}}^{800 \text{ nm}} T(\lambda)S(\lambda)P(\lambda) d\lambda}{\int_{400 \text{ nm}}^{800 \text{ nm}} P(\lambda)S(\lambda) d\lambda} \quad \text{Equation-S4}$$

where λ , $S(\lambda)$, $T(\lambda)$, and $P(\lambda)$ are the wavelength, AM1.5 solar irradiation (100 mW/cm²), transmittance of the ST-PSC, and photopic response of human eyes at wavelength λ .

5. Mott-Schottky (M-S) analysis:

The depletion layer capacitance (C) can be written using the following equation:

$$\frac{1}{C^2} = \frac{-2}{\epsilon\epsilon_0qA^2N} (V - V_{bi}) \quad \text{Equation-S5}$$

Where ϵ , ϵ_0 , A , N , and V_{bi} represents the relative dielectric constant, vacuum permittivity, area of the device, residual charge density and built-in potential, respectively. N can be estimated from the slope of the linearly fit M-S curve.

6. Linear relationship between light intensity and V_{oc} , J_{sc} :

$$\frac{V_{oc}}{\ln\left(\frac{I}{I_0} + 1\right)} = \frac{nk_B T}{q} \quad \text{Equation-S6}$$

where I , I_0 , n , k_B , T and q are light intensity, initial light intensity, ideality factor, Boltzmann constant, absolute temperature, and elementary charge, respectively.

$$J_{sc} \propto I^\alpha \quad \text{Equation-S7}$$

7. Hysteresis index was calculated by the following equation:

$$HI = \frac{PCE_F - PCE_R}{PCE_F} \quad \text{Equation-S8}$$

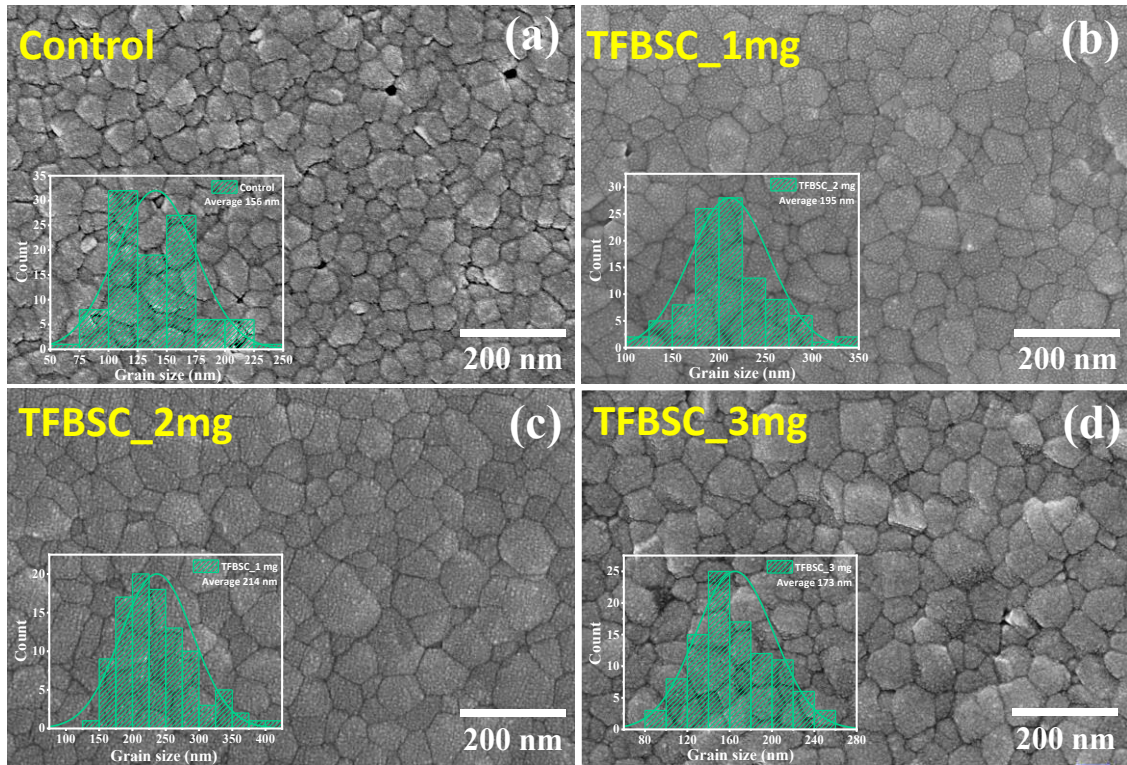


Figure S1. FESEM images of (a) control; (b) 1 mg TFBSC; (c) 2 mg TFBSC; and (d) 3 mg TFBSC-modified semi-transparent perovskite films.

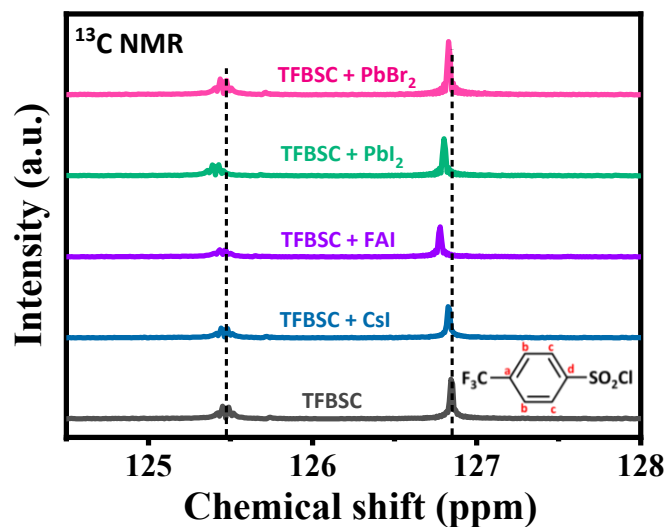


Figure S2. Full range ^{13}C NMR spectra of TFBS-C with CsI, FAI, PbI_2 , and PbBr_2 (inset-molecular structure of TFBS-C).

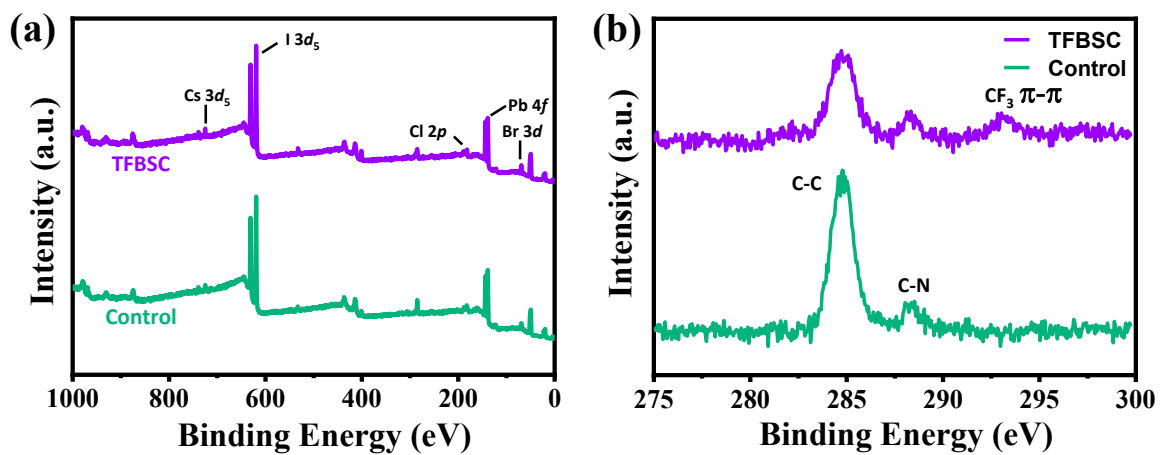


Figure S3. (a) Full range XPS spectra of control and TFBS-C-modified perovskite films; and (b) Core level XPS spectra of C $1s$.

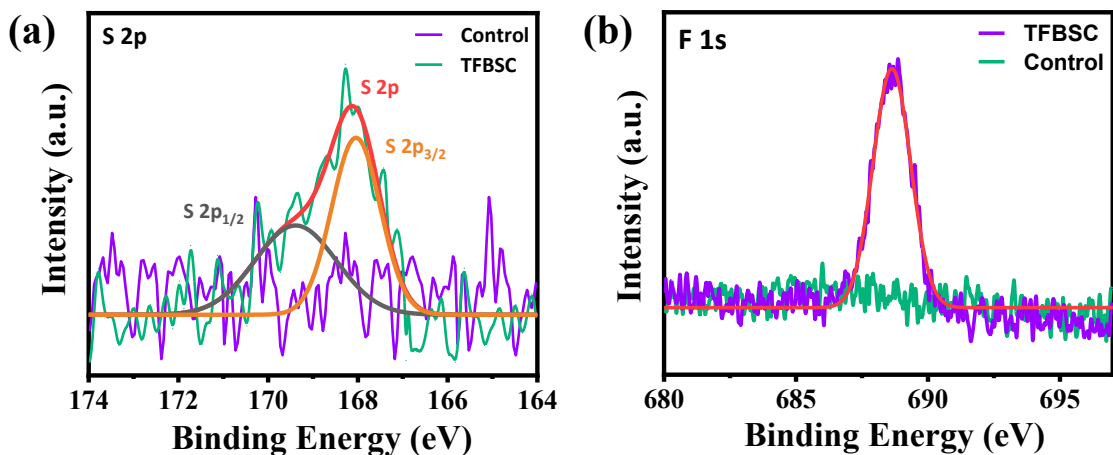


Figure S4. Deconvoluted core level XPS spectra of (a) $S2p$; and (b) $F1s$ of control and TFBSC-modified perovskite films.

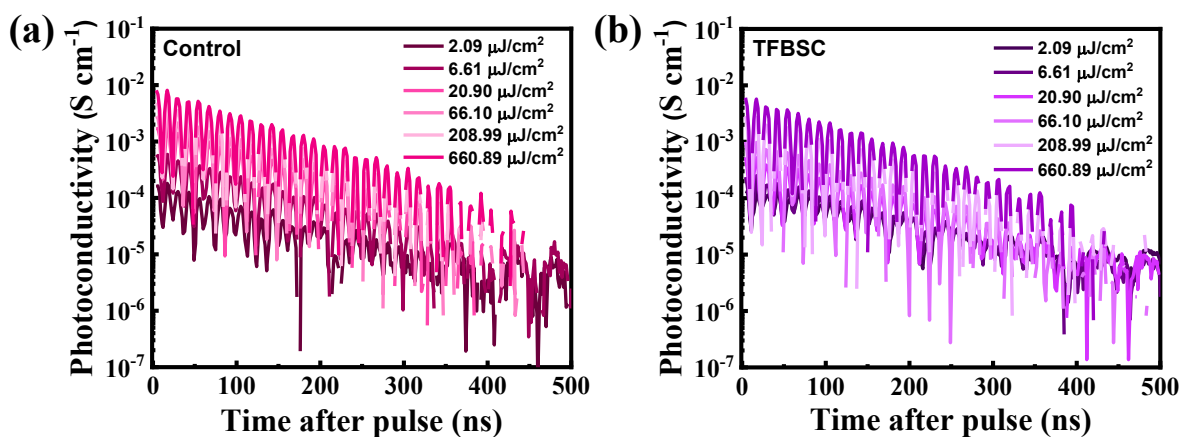


Figure S5. Transient photoconductivity decays of (a) control and (b) TFBSC-modified perovskite films at different excitation fluences from a 470 nm pulsed laser with 10 Hz repetition rate.

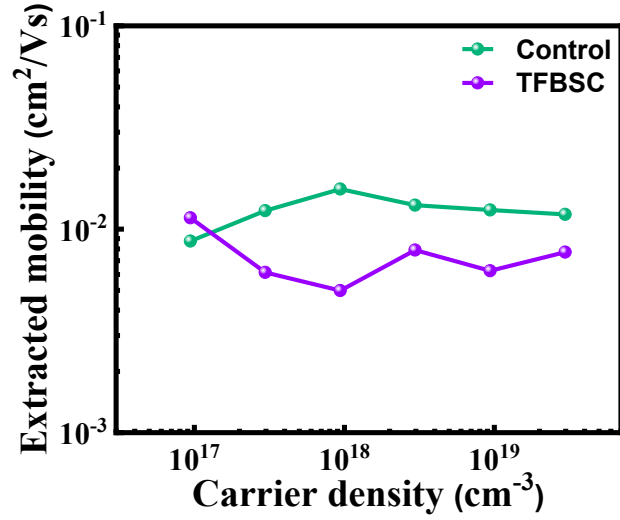


Figure S6. The extracted long-range electron-hole mobility of control and TFBS-modified perovskite films at different excited carrier densities.

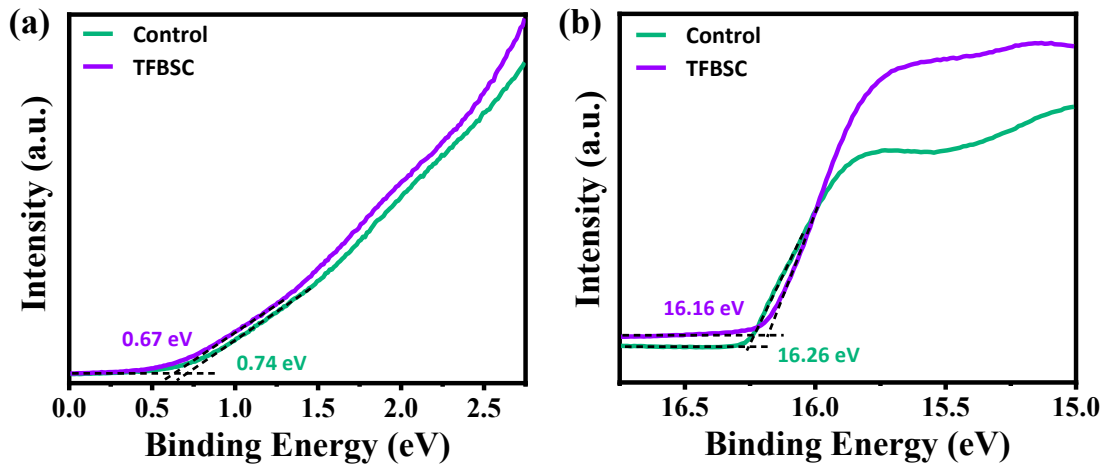


Figure S7. (a,b) UPS spectra of control and TFBS-modified semi-transparent perovskite films.

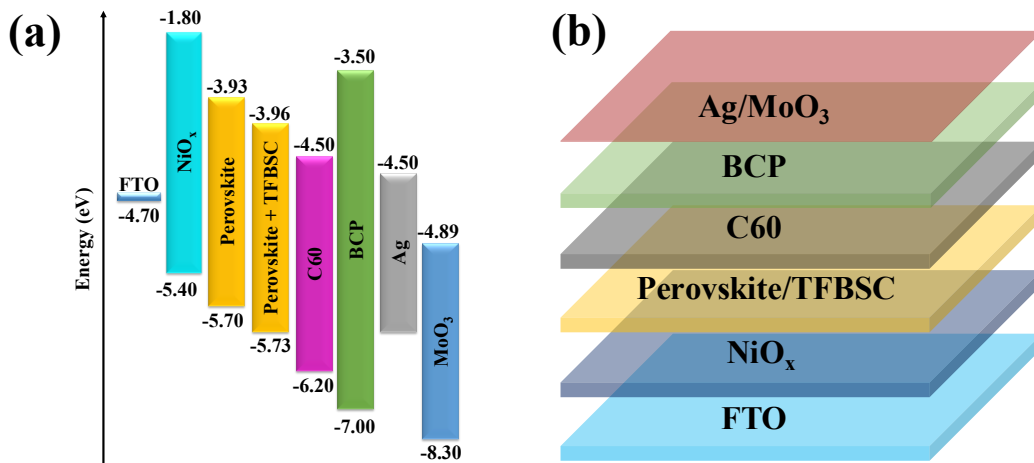


Figure S8. (a) Energy level diagram of the ST-PSCs with and without TFBS-passivation; (b) The device architecture of ST-PSCs.

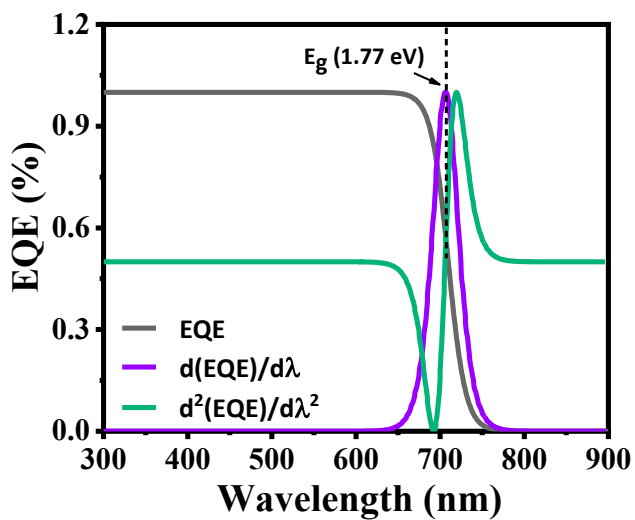


Figure S9. Schematic of band-gap calculation from sigmoidal parameterization of EQE spectra of ST-PSCs.

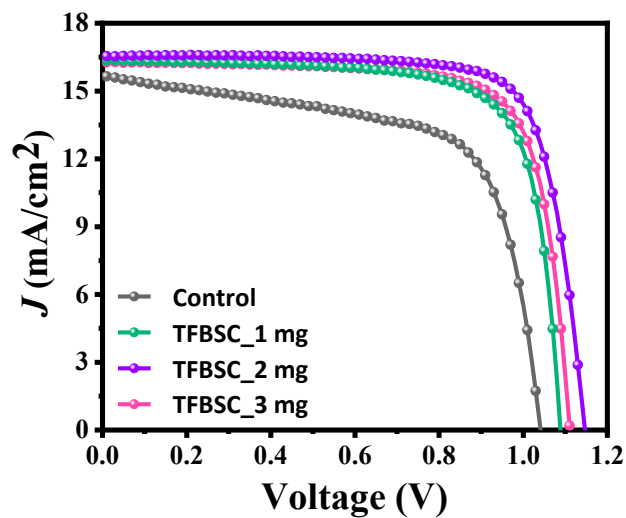


Figure S10. J - V curves of control and modified ST-PSCs with varying concentration of TFBS.

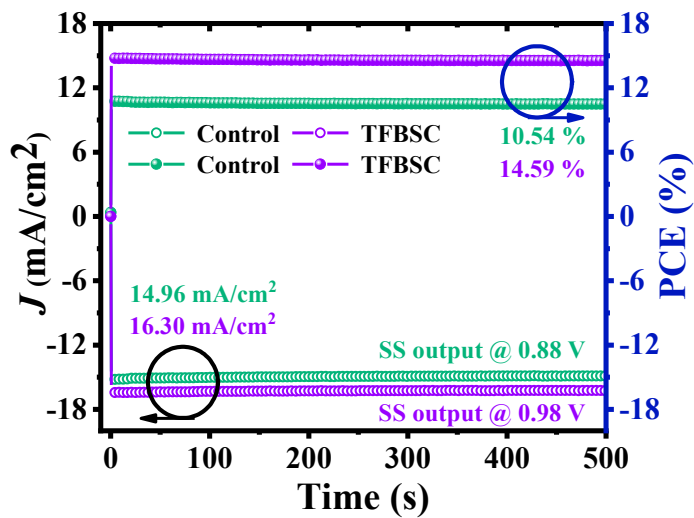


Figure S11. Steady state power output at MPPs of control and TFBS-modified ST-PSCs.

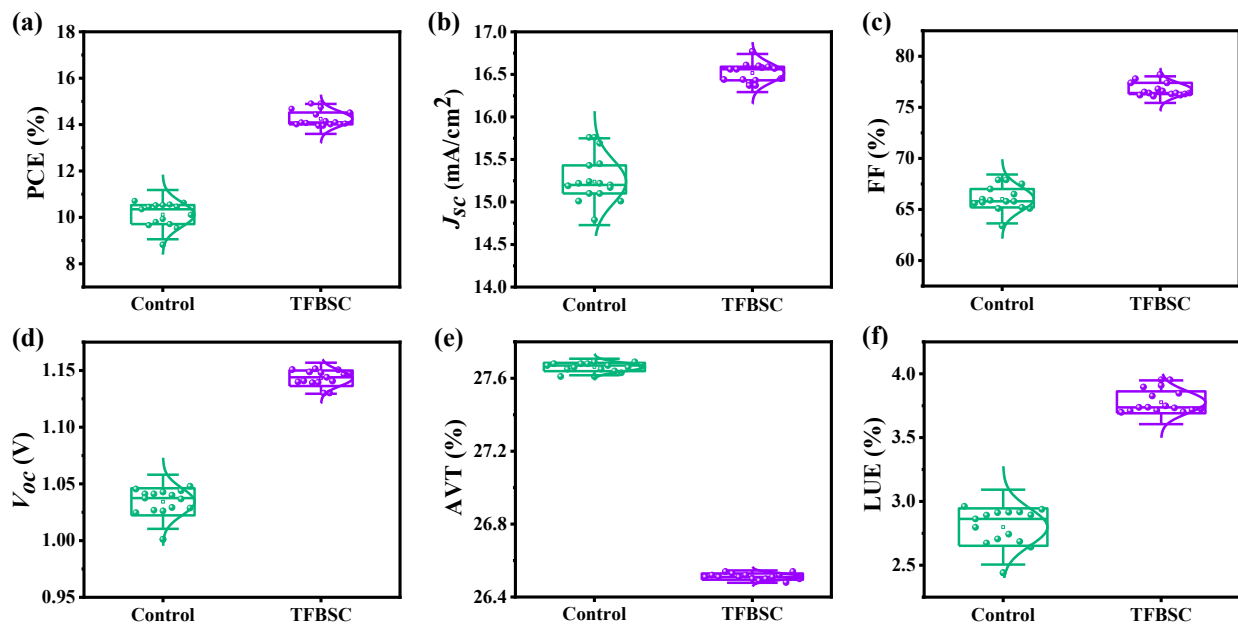


Figure S12. Statistical distribution of 15 devices each for control and TFBS-modified: (a) PCE, (b) J_{sc} , (c) FF, (d) V_{oc} (e) AVT, and (f) LUE.

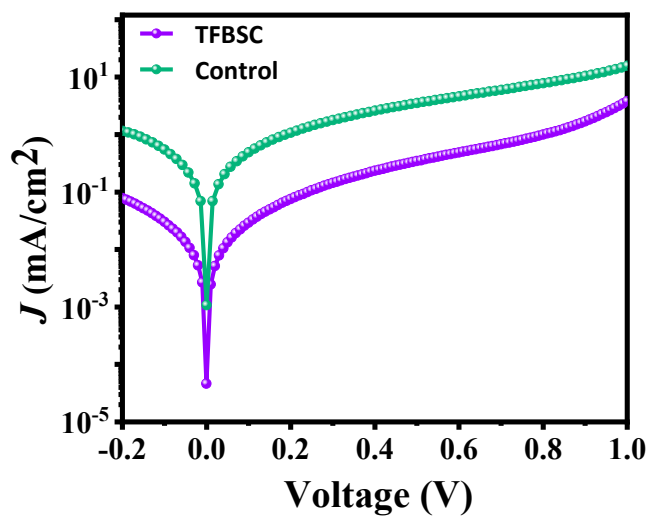


Figure S13. (a) Dark J - V curves for control and TFBS-modified ST-PSCs.

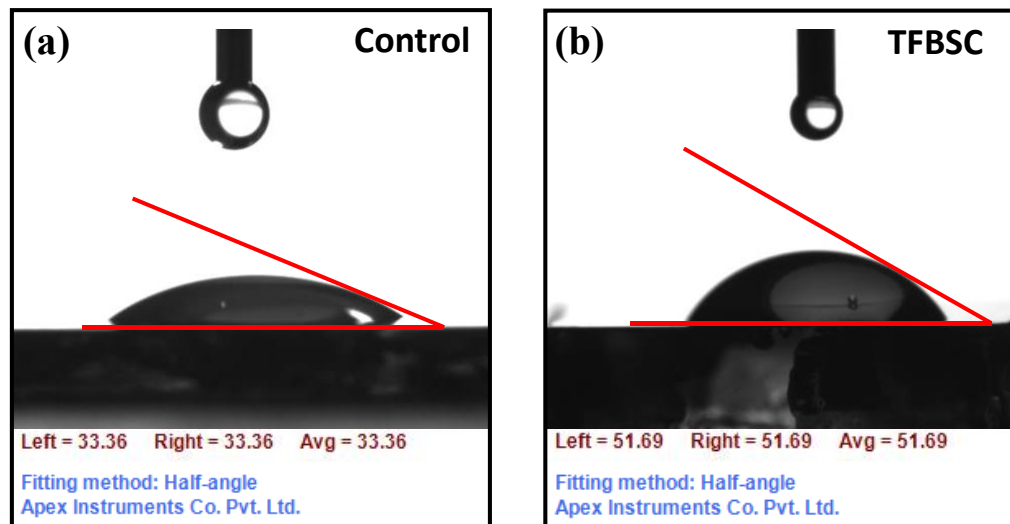


Figure S14. Water contact angles of (a) control and (b) TFBSC-modified perovskite films.

Table S1. TRPL parameters of control and TFBSC-modified devices.

	T_1 (ns)	A_1	T_2 (ns)	A_2	T_{ave} (ns)
Control	51.93	0.440	178.07	0.559	154.52
TFBSC	66.82	0.372	216.22	0.628	189.57

Table S2. Work function (WF) calculated from UPS and KPFM for control and TFBSC-modified devices.

	Control	TFBSC
WF (KPFM)	5.02 eV	5.05 eV
WF (UPS)	4.96 eV	5.06 eV

Table S3. Photovoltaic parameters of ST-PSCs with varying concentration of TFBSC. All the measurements were recorded under 1 sun illumination and 0.1 cm^2 device active area at a scan speed of 10 mV/s.

		PCE (%)	V_{oc} (V)	J_{sc} (mA/cm²)	FF (%)
Control	Max.	10.71	1.04	15.17	67.5
	Ave.	10.38 ± 0.51	1.01 ± 0.02	15.15 ± 0.29	65.31 ± 2.59
TFBSC_1 mg	Max.	13.39	1.08	16.35	75.2
	Ave.	13.14 ± 0.27	1.06 ± 0.03	16.33 ± 0.15	74.04 ± 2.18
TFBSC_2 mg	Max.	14.75	1.15	16.43	78.2
	Ave.	14.61 ± 0.11	1.14 ± 0.01	16.41 ± 0.10	76.73 ± 1.40
TFBSC_3 mg	Max.	14.15	1.12	16.43	78.2
	Ave.	13.85 ± 0.46	1.10 ± 0.03	16.39 ± 0.14	75.98 ± 1.90

Average 15 devices

Table S4. Forward-Reverse photovoltaic parameters of champion devices without and with TFBSC-modifications.

		PCE (%)	V_{oc} (V)	J_{sc} (mA/cm²)	FF (%)	HI (%)
Control	F	10.71	1.04	15.17	67.5	3.36
	R	10.35	1.04	15.10	65.8	
TFBSC	F	14.75	1.15	16.43	78.2	1.55
	R	14.52	1.14	16.37	77.4	

Table S5. EIS parameters of ST-PSCs of control and TFBSC-modified devices.

	R_s (KΩ)	R_{rec} (kΩ)	CPE (nF)
Control	0.602	19.18	23.60
TFBSC	0.481	40.16	15.79

Table S6. A comparison of performance parameters of ST-PSCs with recent literature.

Reference No.	Device Structure	Voc (V)	Jsc (mA/cm ²)	FF (%)	PCE (%)	AVT (%)	LUE (%)	Year
1	FTO/c-TiO ₂ /m-TiO ₂ /perovskite/Carbon	0.79	24.82	—	5.60	8.65	0.48	2024
2	IZO/PEDOT: PSS/MAPbI ₃ /C ₆₀ /BCP/thin Ag	0.92	8.68	71.50	5.70	21.50	1.22	2024
3	ITO/SnO ₂ /(Cs _{0.05} MA _{0.02} FA _{0.93} Pb(I _{0.98} Br _{0.02}) ₃ /thin Au	1.00	15.34	69.09	10.60	25.50	2.70	2024
4	FTO/SnO ₂ /perovskite/2D NPLs -PMMA composite layer/Spiro-OMeTAD/MoO ₃ /Au/MoO ₃	1.07	19.81	67.28	14.26	19.40	2.76	2024
5	FTO/NiO _x /Cs _{0.1} FA _{0.9} PbI ₂ Br +TABr/PCBM/Rhodamine/Ag/MoO _x	1.20	15.92	74.00	14.21	22.00	3.12	2024
6	FTO/SnO ₂ /CsPbBr ₃ /NiO _x /ITO	1.55	6.67	70.00	7.28	44.00	3.20	2024
7	FTO/NiO _x /Cs _{0.1} FA _{0.9} PbI ₂ Br /CPAC/PCBM/Rhodamine/Ag/MoO _x	1.23	15.87	72.70	14.11	24.50	3.45	2024
8	FTO/SnO ₂ /FAPbBr ₃ /PTAA/ITO	1.40	7.35	65.70	6.80	55.00	3.74	2024
9	FTO/Me-4PACz/Cs _{0.05} FA _{0.95} PbI _{2.55} Br _{0.45} /C ₆₀ /thin Ag	1.24	9.8	80.70	10.01	51.05	5.11	2024
10	ITO/SnO ₂ /Perovskite/Spiro OMeTAD/MoO ₃ /Au/Ag/MoO ₃	1.21	19.81	74.89	18.00	17.97	3.23	2025
11	FTO/c-TiO ₂ /CsPbBr ₃ /PTAA/ITO	1.55	6.30	62.46	6.1	58.00	3.53	2025
12	ITO/NiO _x /Me-4PACz/perovskite/2-TEAI/C ₆₀ /BCP/thin Ag	1.18	21.03	75.46	18.73	20.71	3.87	2025
This Work	FTO/NiO_x/Cs_{0.1}FA_{0.9}PbI₂Br +TFBSC/C₆₀/BCP/Ag/MoO₃	1.15	16.43	78.20	14.75	26.58	3.92	2025

References:

- (1) Khan, A. D.; Basit, A.; Rehman, Q.; Noman, M.; Ahmad, M. S.; Wali, Q.; Amir, M.; Khan, A. D. Innovative designs for semitransparent carbon-based perovskite solar cells for building-integrated applications. *Solar Energy* **2024**, *282*, 112951. DOI: <https://doi.org/10.1016/j.solener.2024.112951>.
- (2) Przepis, Ł.; Żuraw, W.; Grodzicki, M.; Ścigaj, M.; Kudrawiec, R.; Herman, A. P. Facile Preparation of Large-Area, Ultrathin, Flexible Semi-Transparent Perovskite Solar Cells via Spin-Coating. *ACS Applied Energy Materials* **2024**, *7* (11), 4803-4812. DOI: 10.1021/acsaem.4c00517.
- (3) Alkhudhari, O. M.; Wang, R.; Jia, Z.; Hodson, N. W.; Alruwaili, A.; Altujjar, A.; Picheo, E.; Saunders, B. R. Structurally colored semitransparent perovskite solar cells using one-step deposition of self-ordering microgel particles. *RSC Advances* **2024**, *14* (9), 6190-6198, 10.1039/D4RA00324A. DOI: 10.1039/D4RA00324A.
- (4) Yang, Y.; Hoang, M. T.; Chiu, W.-H.; Yu, Y.; Wang, H. Efficient Bifacial Semitransparent Perovskite Solar Cells Using Down-Conversion 2D Perovskite Nanoplatelets–Poly(Methyl Methacrylate) Composite Film. *Small Structures* **2024**, *5* (6), 2300547. DOI: <https://doi.org/10.1002/sstr.202300547> (accessed 2025/04/29).
- (5) Garai, R.; Sharma, B.; Afroz, M. A.; Choudhary, S.; Sharma, T.; Metcalf, I.; Tailor, N. K.; Iyer, P. K.; Mohite, A. D.; Satapathi, S. High-Efficiency Semitransparent Perovskite Solar Cells Enabled by Controlling the Crystallization of Ultrathin Films. *ACS Energy Letters* **2024**, *9* (6), 2936-2943. DOI: 10.1021/acsenergylett.4c01149.
- (6) Jiang, X.; Geng, C.; Yu, X.; Pan, J.; Zheng, H.; Liang, C.; Li, B.; Long, F.; Han, L.; Cheng, Y.-B.; et al. Doping with KBr to Achieve High-Performance CsPbBr₃ Semitransparent Perovskite Solar Cells. *ACS Applied Materials & Interfaces* **2024**, *16* (15), 19039-19047. DOI: 10.1021/acsaami.4c02402.
- (7) Sharma, B.; Garai, R.; Afroz, M. A.; Sharma, T.; Choudhary, S.; Singh, R. K.; Satapathi, S. Enhancing Light Utilization Efficiency of Semi-Transparent Perovskite Solar Cells via Tailored Interfacial Engineering. *Advanced Energy Materials* **2024**, *14* (39), 2402473. DOI: <https://doi.org/10.1002/aenm.202402473> (accessed 2025/04/23).
- (8) Jafarzadeh, F.; Castriotta, L. A.; Legrand, M.; Ory, D.; Cacovich, S.; Skafi, Z.; Barichello, J.; De Rossi, F.; Di Giacomo, F.; Di Carlo, A.; et al. Flexible, Transparent, and Bifacial Perovskite Solar Cells and Modules Using the Wide-Band Gap FAPbBr₃ Perovskite Absorber. *ACS Applied Materials & Interfaces* **2024**, *16* (14), 17607-17616. DOI: 10.1021/acsaami.4c01071.
- (9) Shrivastav, N.; Wadhwa, G.; Mani, P.; Madan, J.; Pandey, R. New absorbent layer through employing semi-transparent Cs_{0.05}FA_{0.95}Pb_{1.55}Br_{0.45} in perovskite solar cells for solar windows: Balancing efficiency and transparency. *Materials Letters* **2024**, *377*, 137553. DOI: <https://doi.org/10.1016/j.matlet.2024.137553>.
- (10) Cui, X.; Li, X.; Wang, Z.; Li, Z.; Chen, X.; Tang, J.; Feng, X.; La, S.; Chen, J.; Zhang, Z.; et al. MoO₃/Au/Ag/MoO₃ multilayer transparent electrode enables high light utilization of semitransparent perovskite solar cells. *Device* **2025**, *3* (1). DOI: 10.1016/j.device.2024.100558 (accessed 2025/04/29).
- (11) Barichello, J.; Paci, B.; Moras, P.; Hajhemati, J.; Generosi, A.; Riva, F. R.; Cacovich, S.; Jafarzadeh, F.; Brunetti, F.; Carlo, A. D.; et al. Exploiting the impact of Ionic Liquids and light exposure on performance of fully inorganic CsPbBr₃ semi-transparent perovskite solar cells. *Solar Energy* **2025**, *287*, 113237. DOI: <https://doi.org/10.1016/j.solener.2024.113237>.
- (12) Chen, D.; Shi, W.; Gao, Y.; Wang, S.; Tian, B.; Wang, Z.; Zhu, W.; Zhou, L.; Xi, H.; Dong, H.; et al. Fabrication of Bifacial-Modified Perovskites for Efficient Semitransparent Solar Cells with High Average Visible Transmittance. In *Molecules*, 2025; Vol. 30, p 1237.